Video Article

Scalable Solution-processed Fabrication Strategy for High-performance, Flexible, Transparent Electrodes with Embedded Metal Mesh

Arshad Khan[1], Sangeon Lee[2], Taehee Jang[3], Ze Xiong[4], Cuiping Zhang[1,5], Jinyao Tang[4], L. Jay Guo[2,3], Wen-Di Li[1,5]

[1]Department of Mechanical Engineering, University of Hong Kong

[2]Department of Mechanical Engineering, University of Michigan

[3]Department of Electrical Engineering and Computer Science, University of Michigan

[4]Department of Chemistry, University of Hong Kong

[5]HKU-Shenzhen Institute of Research and Innovation

Correspondence to: Wen-Di Li at liwd@hku.hk

URL: https://www.jove.com/video/56019
DOI: doi:10.3791/56019

Keywords: Engineering, Issue 124, Embedded metal mesh, flexible transparent electrode, solution-processed, lithography, electrodeposition, thermal imprint transfer

Date Published: 6/23/2017

Citation: Khan, A., Lee, S., Jang, T., Xiong, Z., Zhang, C., Tang, J., Guo, L.J., Li, W.D. Scalable Solution-processed Fabrication Strategy for High-performance, Flexible, Transparent Electrodes with Embedded Metal Mesh. *J. Vis. Exp.* (124), e56019, doi:10.3791/56019 (2017).

Abstract

Here, the authors report the embedded metal-mesh transparent electrode (EMTE), a new transparent electrode (TE) with a metal mesh completely embedded in a polymer film. This paper also presents a low-cost, vacuum-free fabrication method for this novel TE; the approach combines lithography, electroplating, and imprint transfer (LEIT) processing. The embedded nature of the EMTEs offers many advantages, such as high surface smoothness, which is essential for organic electronic device production; superior mechanical stability during bending; favorable resistance to chemicals and moisture; and strong adhesion with plastic film. LEIT fabrication features an electroplating process for vacuum-free metal deposition and is favorable for industrial mass production. Furthermore, LEIT allows for the fabrication of metal mesh with a high aspect ratio (*i.e.,* thickness to linewidth), significantly enhancing its electrical conductance without adversely losing optical transmittance. We demonstrate several prototypes of flexible EMTEs, with sheet resistances lower than 1 Ω/sq and transmittances greater than 90%, resulting in very high figures of merit (FoM) – up to 1.5 x 10^4 – which are amongst the best values in the published literature.

Video Link

The video component of this article can be found at https://www.jove.com/video/56019/

Introduction

Worldwide, studies are being conducted to look for replacements for rigid transparent conductive oxides (TCOs), such as indium tin oxide and fluorine-doped tin oxide (FTO) films, in order to fabricate flexible/stretchable TEs to be used in future flexible/stretchable optoelectronic devices[1]. This necessitates novel materials with new fabrication methods.

Nanomaterials, such as graphene[2], conducting polymers[3,4], carbon nanotubes[5], and random metal nanowire networks[6,7,8,9,10,11], have been studied and have demonstrated their capabilities in flexible TEs, addressing the shortcomings of existing TCO-based TEs, including film fragility[12], low infrared transmittance[13], and low abundance[14]. Even with this potential, it is still challenging to attain high electrical and optical conductance without deterioration under continuous bending.

In this framework, regular metal meshes[15,16,17,18,19,20] are evolving as a promising candidate and have accomplished remarkably high optical transparency and low sheet resistance, which can be tunable on demand. However, the extensive use of metal mesh-based TEs has been hindered due to numerous challenges. First, fabrication often involves the expensive, vacuum-based deposition of metals[16,17,18,21]. Second, the thickness may easily cause electrical short-circuiting[22,23,24,25] in thin-film organic optoelectronic devices. Third, the weak adhesion with the substrate surface results in poor flexibility[26,27]. The abovementioned limitations have created a demand for novel metal mesh-based TE structures and scalable approaches for their fabrication.

In this study, we report a novel structure of flexible TEs that contains a metal mesh completely embedded in a polymer film. We also describe an innovative, solution-based, and low-cost fabrication approach that combines lithography, electrodeposition, and imprint transfer. FoM values as high as 15k have been achieved on sample EMTEs. Due to the embedded nature of EMTEs, remarkable chemical, mechanical, and environmental stability were observed. Furthermore, the solution-processed fabrication technique established in this work can potentially be used for the low-cost and high-throughput production of the proposed EMTEs. This fabrication technique is scalable to finer metal-mesh linewidths, larger areas, and a range of metals.

Protocol

CAUTION: Please pay attention to electron beam safety. Please wear the correct protective glasses and clothes. Also, handle the all flammable solvents and solutions carefully.

1. Photolithography-based Fabrication of the EMTE

1. **Photolithography for fabricating the mesh pattern.**
    1. Clean FTO glass substrates (3 cm x 3 cm) with liquid detergent using cotton swab. Rinse them thoroughly with deionized (DI) water using a clean cotton swab. Further clean them using ultra-sonication (frequency = 40 kHz, temperature = 25 °C) in isopropyl alcohol (IPA) for 30 s before drying them with compressed air.
    CAUTION: Handle compressed air carefully.
    2. Spincoat 100 µL of the photoresist on the cleaned FTO glass for 60 s at 4,000 rpm (approximately 350 x g for samples with a 2 cm radius) to get a 1.8 µm-thick, uniform film.
    3. Bake the photoresist film on a hotplate for 50 s at 100 °C.
    4. Expose the photoresist film through a photomask with a mesh pattern (3 µm linewidth, 50 µm pitch) using a UV mask aligner for a dose of 20 mJ/cm^2.
    5. Develop the photoresist by immersing the sample in the developer solution for 50 s.
    6. Rinse the sample in DI water and dry it with compressed air.
    CAUTION: Handle compressed air carefully.

2. **Electrodeposition of metals.**
    1. Pour 100 mL of copper aqueous plating solution in a 250 mL beaker.
    NOTE: Other aqueous plating solutions (*e.g.,* silver, gold, nickel, and zinc) can be used for the fabrication of EMTEs with the respective metals.
    CAUTION: Pay attention to chemical safety.
    2. Connect the photoresist-covered FTO glass to the negative terminal of the two-electrode electrodeposition setup and immerse it in the plating solution as the working electrode.
    3. Connect the copper metal bar to the positive terminal of the two-electrode electrodeposition setup as the counter electrode.
    4. Supply a constant 5-mA current (current density: ~3 mA/cm^2) using a voltage/current sourcing and measurement instrument (*e.g.* Sourcemeter) for 15 min to deposit the metal to a thickness of approximately 1.5 µm.
    5. Thoroughly rinse the photoresist-coated FTO glass sample with DI water and dry it with compressed air.
    CAUTION: Handle compressed air carefully.
    6. Place the photoresist-coated FTO glass sample in acetone for 5 min to dissolve the photoresist film, with the bare metal mesh on top of the FTO glass.

3. **Thermal imprint transfer of the metal mesh to the flexible substrate.**
    1. Place the metal mesh-covered FTO glass sample onto the electrically heated platens of the thermal imprinter and put a 100 µm-thick flexible cyclic olefin copolymer (COC) film on top of the sample, facing the metal mesh side.
    2. Heat the plates of the heated press to 100 °C.
    3. Apply 15 MPa of imprint pressure and hold it for 5 min.
    CAUTION: Pay attention to safety when using the heated press.
    NOTE: The imprint transfer can be done at a lower pressure; the pressure value (15 MPa) reported here is relatively high. This high pressure was used to ensure that the metal mesh was fully embedded in the COC film.
    4. Cool the heated platens to the demolding temperature of 40 °C.
    5. Release the imprint pressure.
    6. Peel off the COC film from the FTO glass, with the metal mesh entirely embedded in the COC film.

2. Fabrication of Sub-micron EMTEs

1. **Fabrication of sub-micron EMTEs using electron beam lithography (EBL).**
    1. Spincoat 100 µL of polymethyl methacrylate (PMMA) solution (15k M.W., 4 wt. % in anisole) on the cleaned FTO glass for 60 s at 2,500 rpm (approximately 140 x g for samples with a 2 cm radius) to achieve a 150 nm-thick, uniform film.
    2. Bake the PMMA film on a hotplate for 30 min at 170 °C.
    3. Turn on the EBL system and design the mesh pattern (400-nm linewidth, 5 µm pitch) using a pattern generator[29].
    4. Place the sample in a scanning electron microscope connected to the pattern generator and execute the writing process[29].
    5. Develop the resist for 60 s in a mixed solution of methyl isopropyl ketone and isopropanol at a 1:3 ratio.
    6. Rinse the sample with DI water and dry it with compressed air.
    CAUTION: Handle compressed air carefully.
    7. Place 100 mL of the copper aqueous plating solution in a medium-size beaker.
    NOTE: Other aqueous plating solutions (*e.g.,* silver, gold, nickel, and zinc plating solutions) should be used for the fabrication of EMTEs with the respective metals.
    8. Attach the PMMA-coated FTO glass to the negative terminal of the two-electrode electrodeposition setup, dip it in the plating solution as the working electrode, and connect the copper metal bar to the positive terminal to complete the circuit.
    NOTE: Other metals bars (*i.e.,* silver, gold, nickel, and zinc) should be used for the respective metal electrodepositions.

9. Apply a suitable current, corresponding with a current density of approximately 3 mA/cm^2, to the mesh pattern region for 2 min to deposit metal to a thickness of approximately 200 nm (the actual thickness must be determined by SEM or AFM).
10. Carefully wash the sample with DI water and place it in acetone for 5 min to dissolve the PMMA film.
11. Put the metal mesh-covered FTO glass sample on the electrically heated platens of the thermal imprinter and place a COC film (100 µm-thick) on top of the sample.
12. Heat the plates to 100 °C, apply a 15 MPa imprint pressure, and hold it for 5 min.
13. Cool the heated platens to the demolding temperature of 40 °C and release the imprint pressure.
14. Peel off the COC film from the FTO glass, along with thesub-micron metal mesh completely embedded in the COC film.

3. Performance Measurement of the EMTEs

1. **Sheet resistance measurement.**
   1. Spread silver paste on two opposite edges of the square sample and wait until it dries.
   2. Carefully place the four probes of the resistance measurement device on the silver pads, following the equipment instructions.
   3. Switch to the resistance measurement mode of the power source/measurement instrument and record the value on the display.

2. **Optical transmission measurement.**
   1. Turn on the UV-Vis measurement setup and calibrate the spectrometer (*i.e.,* correlate the readings with a standard sample to check the accuracy of the instrument).
   2. Place the EMTE sample on the spectrometer sample holder and properly align the optical direction.
   3. Adjust the spectrometer for 100% transmittance.
      NOTE: All transmittance values presented here are normalized to the absolute transmittance through the bare COC film substrate.
   4. Measure the transmittance of the sample.
   5. Save the measurement and logout of the setup.

Representative Results

Figure 1 displays the schematic and fabrication flowchart of the EMTE samples. As presented in **Figure 1a**, the EMTE consists of a metal mesh fully embedded in a polymer film. The upper face of the mesh is on the same level as the substrate, displaying a generally smooth platform for subsequent device production. The fabrication technique is schematically explained in **Figure 1b**-**e**. After spincoating a photoresist film on an FTO glass substrate, photolithography is used to create the mesh pattern in photoresist by UV exposure and development (**Figure 1b**), revealing the conductive surface of the glass in the trench. In the following step, the respective metal is grown inside the trenches by electrodeposition, which fills the trenches to form a regular metal mesh (**Figure 1c**). Then, the photoresist is carefully removed in acetone, resulting in a weakly attached metal mesh on the surface of the FTO glass (**Figure 1d**). Next, a polymer film is positioned on the sample and heated to a temperature higher than its glass transition temperature. Metal mesh is pushed into the softened polymer film through the application of a uniform pressure (**Figure 1e**). Finally, by cooling the stack to room temperature and peeling off the polymer film from the conductive glass, the metal mesh is transferred to the plastic film in fully embedded form (**Figure 1f**). The entire fabrication procedure is solution-based and is implemented in an ambient atmosphere; therefore, it can easily be adapted for mass production.

Figure 2 presents atomic force microscopy (AFM) and scanning electron microscopy (SEM) images of the morphology of the EMTE at different fabrication steps of the LEIT process. **Figure 2a** presents the trench images in the photoresist film made by photolithography. In this specific sample, the width of the photoresist trench is about 4 µm, while the depth is nearly 2 µm. **Figure 2b** shows the electroplated copper mesh on FTO glass. As apparent from the results, the copper mesh has a thickness and linewidth of about 1.8 and 4 µm, respectively. **Figure 2c** displays the transferred copper mesh on a COC film[28]. The AFM images confirm that the surface roughness of the accomplished EMTE (1.8 µm thickness) is lower than 50 nm, confirming its embedded configuration. The LEIT method can be further studied by varying the electrodeposition time to make copper EMTEs of different thicknesses. The correlation of metal thickness and electrodeposition time is presented in **Figure 2d**.The curve shown in **Figure 2d** reveals that the thickness of metal changes nonlinearly with an increase in electrodeposition time. This is because of the non-rectangular cross-section of the photoresist trench (**Figure 2a**), which has a narrower bottom but a wider top. Thus, during electrodeposition (constant current), the rate of growth of metal thickness decreases with time. Hence, the mesh has a larger width at the higher part, which is advantageous for imprint transfer since it can be mechanically anchored in the plastic film.

Figure 3a-c demonstrates the structural characterization of EBL-patterned EMTE manufacturing at various steps of the LEIT process to validate its dimensional scalability. **Figure 3a** shows the AFM and SEM images of the trenches made in PMMA film via EBL. The trench depth and width are around 150 and 400 nm, respectively. **Figure 3b** shows the copper mesh electroplated on FTO glass, and **Figure 3c** presents the imprint-transferred copper mesh on a COC film. The metal mesh on the COC substrate is in completely embedded form,offering strong adhesion and stability with the plastic substrate.

Figure 4a shows the transmittance of copper EMTEs of 600 nm, 1 µm, and 2 µm thicknesses in the wavelength range of 300-850 nm. When the metal mesh thickness increased from 600 nm to 2 µm, only a minimal reduction in transmittance was detected, and this drop is attributed to the nonrectangular profile of the trench in the photoresist and the metal overplating. On the other hand, the sheet resistance of EMTEs can be significantly decreased when the metal thickness is increased, as demonstrated in **Figure 4b**. An exceptionally low sheet resistance of 0.07 Ω/sq has been recorded for the copper EMTE with a 2-µm thickness, with the optical transmittance still higher than 70%.

Figure 4b exhibits the ratio of electrical conductance to optical conductance (σ_{dc}/σ_{opt}), a FoM commonly used to compare the performance of TEs. The FoM values shown in **Figure 4b** were calculated for various EMTEs made in this work by applying the following commonly used expression[4,7,17,18]:

$$\mathrm{FoM} = \frac{\sigma_{dc}}{\sigma_{opt}} = \frac{188.5}{R_s\left(\frac{1}{\sqrt{T}} - 1\right)}$$

where R_s is the sheet resistance and T is the optical transmittance at a 550-nm wavelength. The inset of **Figure 4b** displays the relationship between the FoM and the metal thickness. The given plot shows that the thickness of the metal has a significant influence on the sheet resistance and therefore on the value of the FoM by enhancing the conductivity of a thicker metal mesh without considerably losing transmittance.The prototype EMTEs attained FoM values higher than 1.5 x 10^4, which are amongst the best values reported in the literature.

Figure 5a demonstrates the sheet resistance and UV-Vis spectra of a high transparent copper EMTE on COC film (5 x 5 cm^2) with a pitch, linewidth, and thickness of 150, 4, and 1 µm, respectively, exhibiting the scalability of the total size of our EMTE structure and LEIT fabrication strategy. Due to the relatively large pitch, the sample displays higher optical transmittance (94%) while maintaining a lower sheet resistance (0.93 Ω/sq). Similarly, numerous arrangements of sheet resistance and optical transmittance can be attained for different devices by adjusting the key geometric characteristics of the EMTE.

Figure 5b shows the sheet resistance and optical transmittance spectra of EMTEs of various metals, including silver, gold, nickel, and zinc, to demonstrate the versatility of material choice with our EMTE. The transmittance spectra are almost flat and featureless over the whole visible range, which is beneficial for display devices and solar cell applications. Zinc-, silver-, and nickel-based EMTEs have comparable metal thicknesses, so all samples have approximately similar transmittances (nearly 78%), while sheet resistances are 1.02, 0.52, and 1.40 Ω/sq, respectively. Due to the different metal thicknesses, the gold- and copper-based EMTEs (nearly 2 µm and 600 nm, respectively) have sheet resistances of 0.20 and 0.70 Ω/sq and transmittances of 72% and 82%, respectively. The successful production of these EMTEs confirmed the material versatility, therefore satisfying diverse requirements for the chemical compatibility and work function of the conductor in various devices.

Figure 6a and b present the superior flexibility of our EMTEs by correlating the sheet resistance with the bending cycles for compressive and tensile loadings at radii of 3, 4, and 5 mm. The results shown in **Figure 6a** demonstrate that, for compressive bending with 4 and 5 mm radii, no obvious variation in sheet resistance (0.07 Ω/sq) occurs for 1,000 bendings. Also, the variation in sheet resistance is within 100% of its initial value (from 0.07 Ω/sq to 0.13 Ω/sq) for the 3 mm bending radius. Similarly, for tensile bending, variations in sheet resistance against the bending cycles are shown in **Figure 6b**, indicating that for 1,000 cycles of 3, 4, and 5 mm radii, the sheet resistances changed by almost 350%, 150%, and 30%, respectively. **Figure 6c** illustrates the environmental stability of the copper EMTEs after immersion in DI water and IPA and exposure to a hot and humid atmosphere (60 °C, 85% relative humidity). It is obvious from the results that after 24 h, the morphological structures and sheet resistances of the EMTEs remain unaffected.

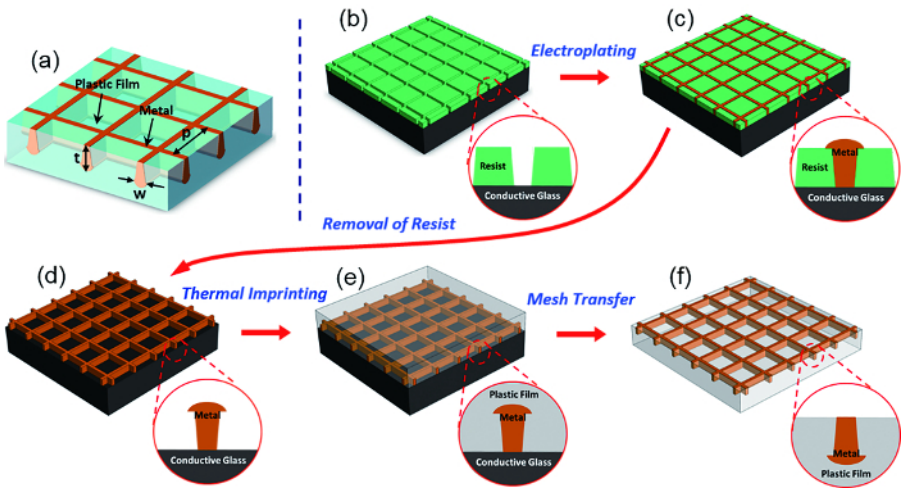

Figure 1: Schematic Diagrams of the EMTE Structure and LEIT Fabrication Procedure. (**a**) An EMTE with a metal mesh embedded in a transparent plastic film. (**b**) Mesh patterns made in a resist film layered on a conductive glass substrate using lithography. (**c**) Electrodeposition of metal inside the trenches of the resist to fabricate a uniform metal mesh. (**d**) Dissolving the resist to achieve bare metal mesh. (**e**) Heating and pressing the metal mesh into a plastic film. (**f**) Separation of the plastic film and the metal mesh in a completely embedded form. This figure has been modified from reference[29]. Please click here to view a larger version of this figure.

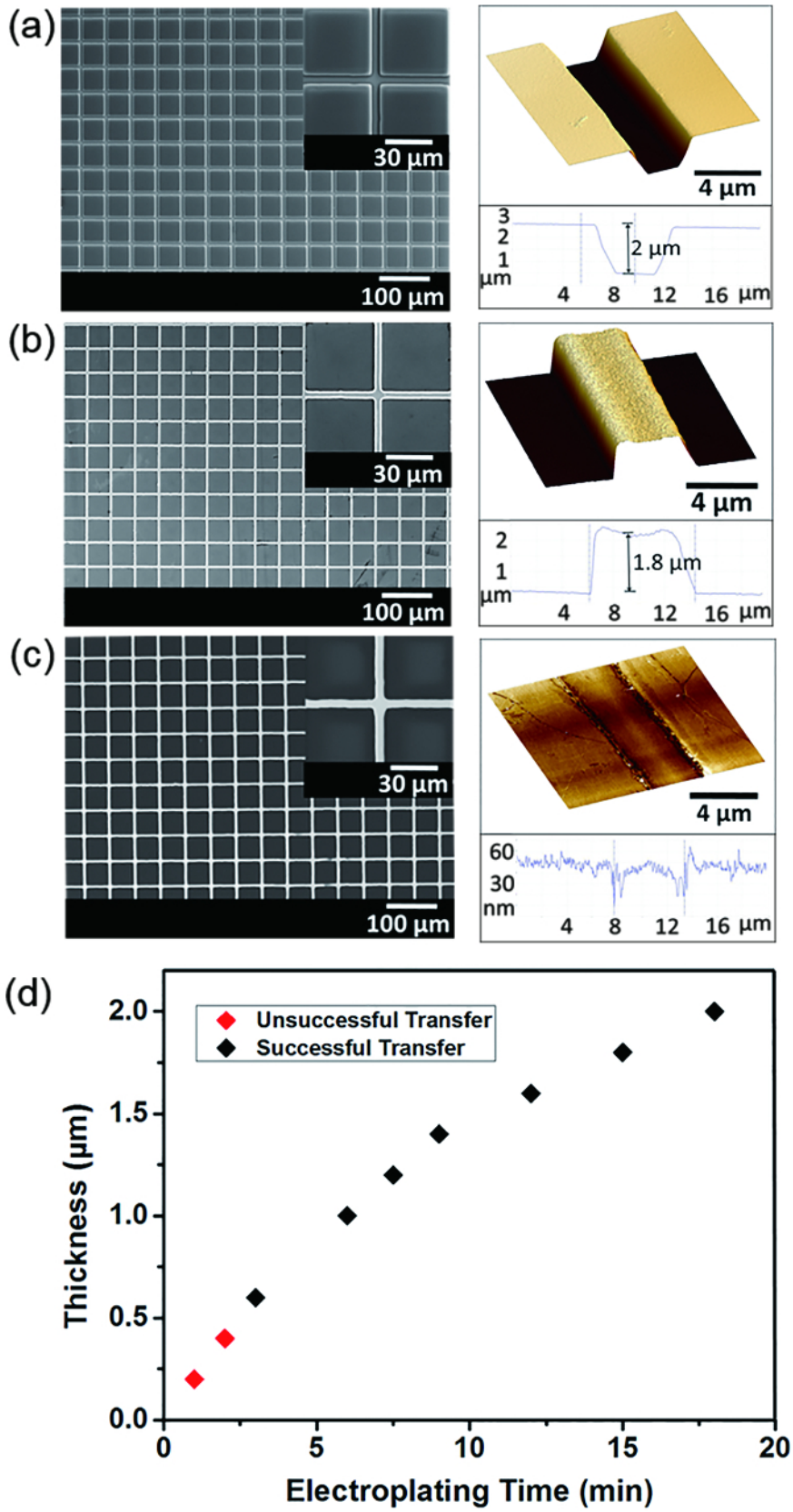

Figure 2: Fabrication of Prototype 50 µm-pitch Copper EMTEs. (**a**-**c**) SEM (left, with the inset showing the zoomed-in image) and AFM (right) characterizations of a sample EMTE at different stages of LEIT: (**a**) Mesh pattern in the photoresist. (**b**) Copper mesh on the FTO glass after dissolving the photoresist. (**c**) Copper mesh completely embedded in a COC substrate. (**d**) Relationship between metal thickness and electrodeposition time at a constant electrodeposition current density (3 mA/cm^2). Unsuccessful and successful cases following the imprint

transfer are denoted by red and black colors, respectively.This figure has been modified from reference[29]. Please click here to view a larger version of this figure.

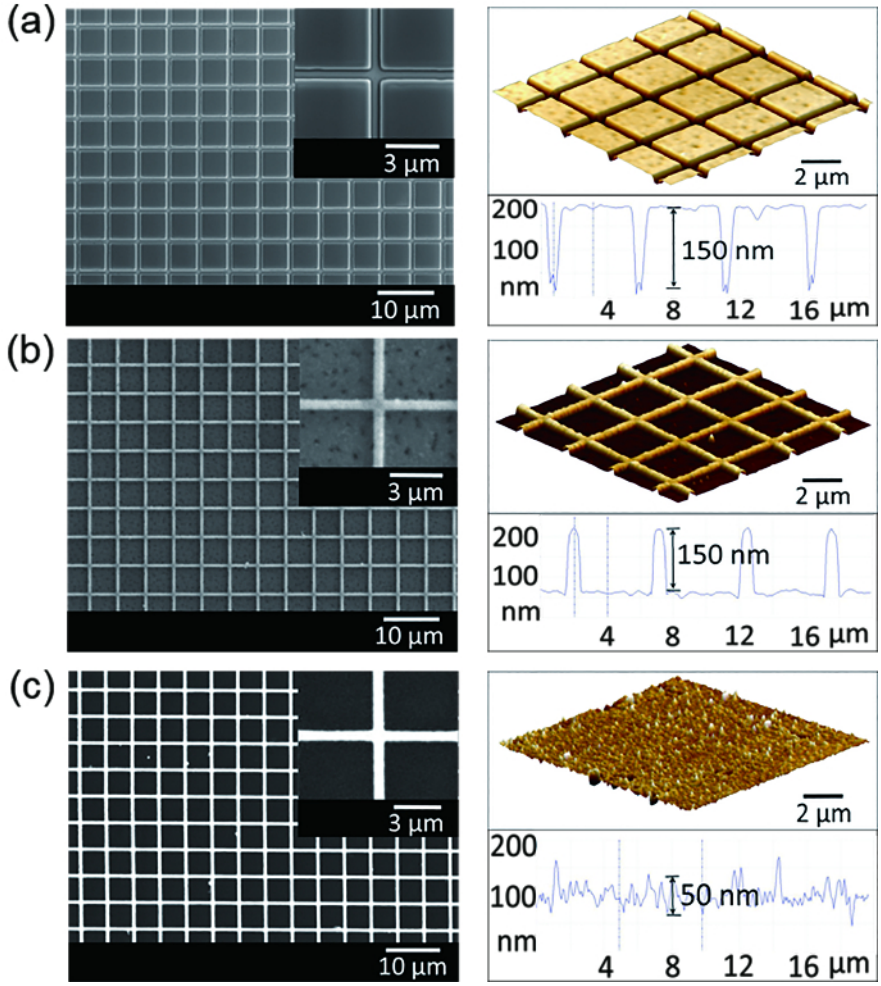

Figure 3: SEM (left) and AFM (right) Characterizations of a Prototype Sub-micrometer-linewidth EMTE at Various Stages of LEIT. (**a**) Nanomesh patterns made in a PMMA film using EBL. (**b**) Copper nanomesh on the FTO glass after dissolving the PMMA film. (**c**) Copper nanomesh completely embedded in a COC substrate. This figure has been modified from reference[29]. Please click here to view a larger version of this figure.

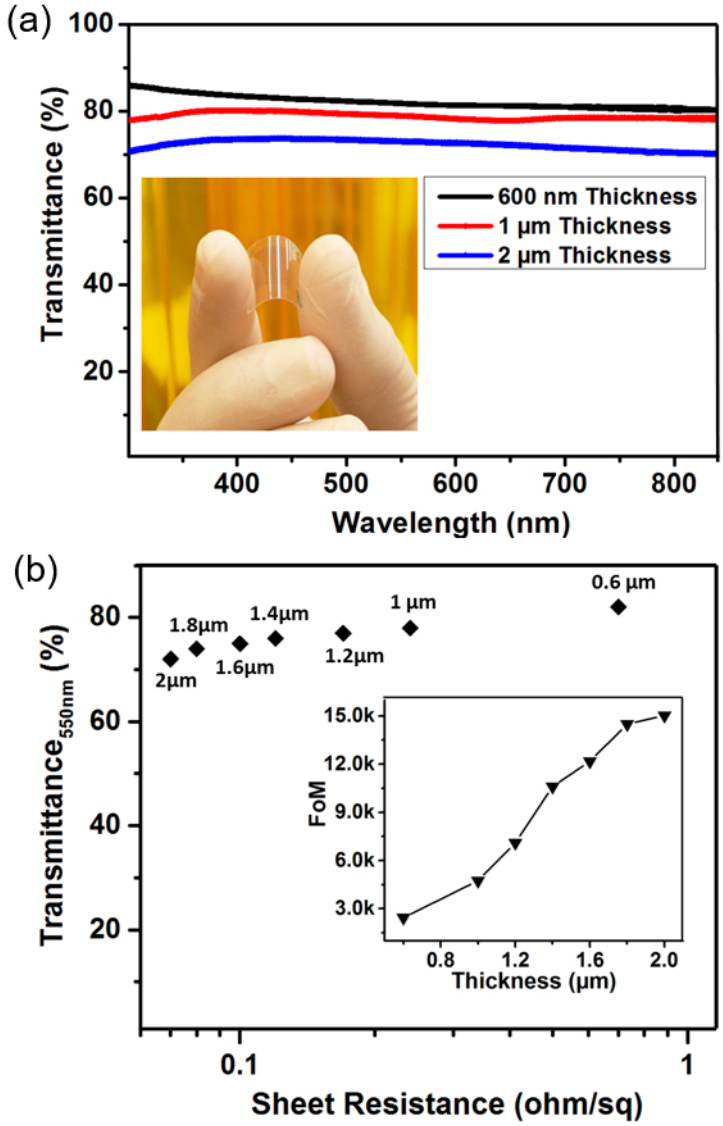

Figure 4: Performance Characterization of the Prototype 50 µm-pitch Copper EMTEs. (**a**) Optical spectra of the typical copper EMTEs. Inset: optical image of the flexible copper EMTE. (**b**) Relationship between transmittance and sheet resistance for copper EMTEs of various mesh thicknesses; the corresponding FoM values are displayed in the inset. This figure has been modified from reference[29]. Please click here to view a larger version of this figure.

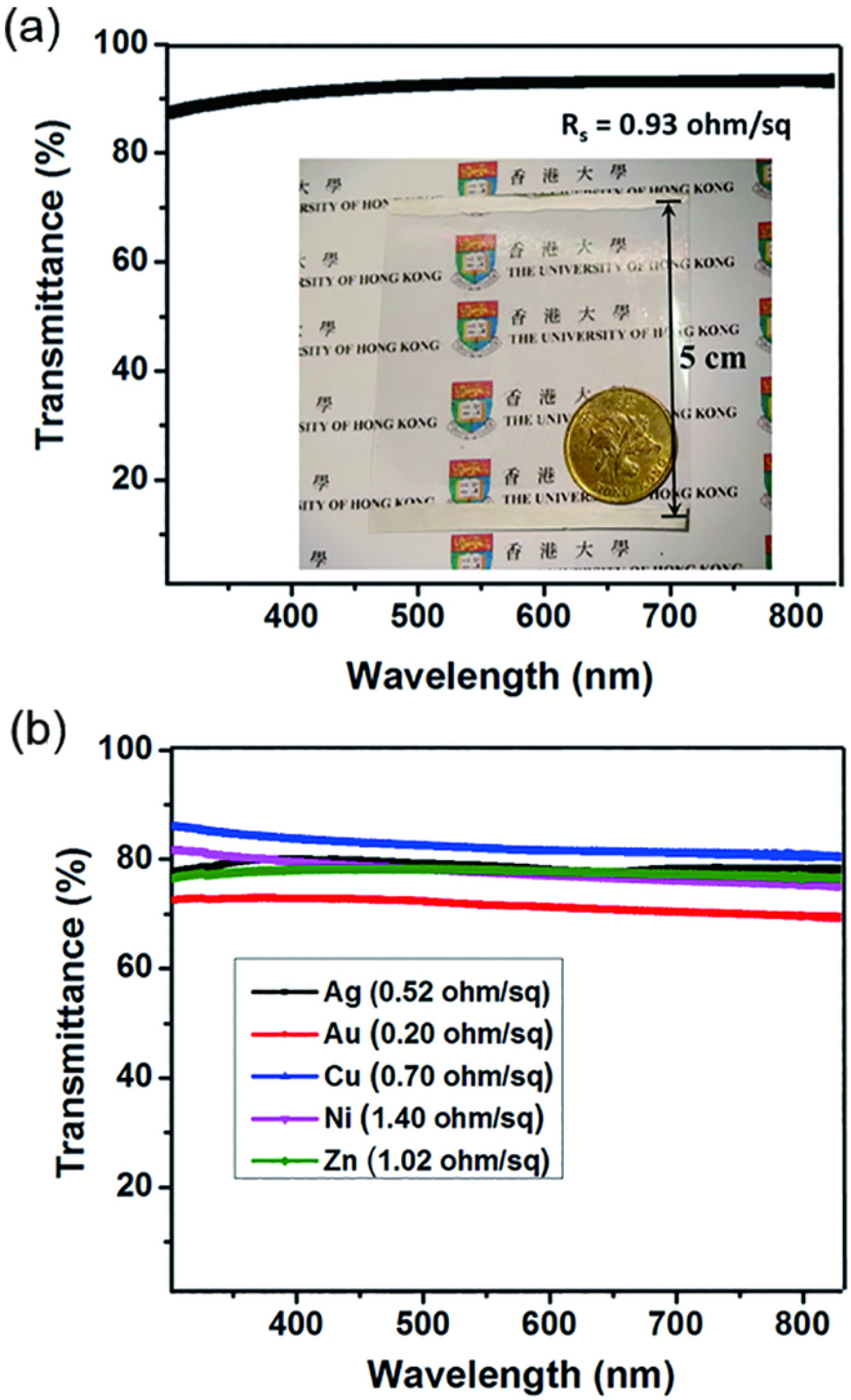

Figure 5: Dimensional Scalability and Material Versatility of the Copper EMTEs. (**a**) Sheet resistance and optical spectra of a high transparent copper EMTE with a pitch of 150 µm on a large COC substrate (5 x 5 cm^2). Inset: optical image of the large-area EMTE. (**b**) Sheet resistances and optical spectra of 50 µm-pitch EMTEs made of different metals. This figure has been modified from reference[29]. Please click here to view a larger version of this figure.

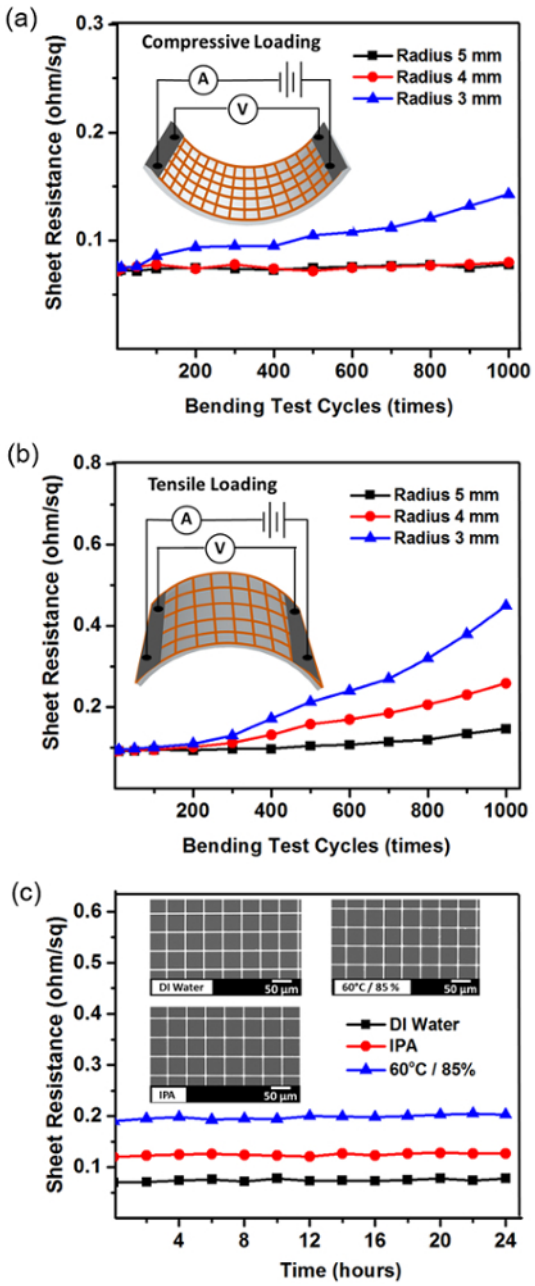

Figure 6: Mechanical and Environmental Stability of the Copper EMTEs. (**a**) Curve of changes in sheet resistance with repeated compressive bending cycles. (**b**) Curve of changes in sheet resistance with repeated tensile bending cycles. (**c**) Changes in sheet resistance in the environmental and chemical tests.Inset: SEM pictures after the tests. This figure has been modified from reference[29]. Please click here to view a larger version of this figure.

Discussion

Our fabrication method can be further modified to allow for scalability of the feature sizes and areas of the sample and for the use of various materials. The successful fabrication of sub-micrometer-linewidth **(Figure 3a-3c**) copper EMTEs using EBL proves that EMTE structure and key steps in LEIT fabrication, including electroplating and imprint transfer, can be reliably scaled down to a sub-micrometer range. Similarly, other large-area lithography processes, such as phase-shift photolithography[30], nanoimprint lithography[31], and charged-particle beam lithography[32], can also be used to create high-resolution patterns in the resist film. The electrodeposition process used in our demonstration is based on a laboratory-scale setup. However, our method can be readily modified to an industrial-scale, large-throughput electroplating bath for production. We used thermal imprint transfer in the demonstration, but other materials that can be cured by ultraviolet or other means can also be applied to the transfer process.

When carrying out our method, some problems may occur. The metal mesh thickness, as well as its geometric profile, are critical for the consistent LEIT fabrication of EMTEs. The curve shown in **Figure 2d** reveals that the transfers were successful only for thicker meshes (*i.e.,* a

thickness greater than 500 nm). The reason for the unsuccessful transfers is that the applied trapping force of the COC film on the upper surface and sidewall of thinner metal meshes simply could not counter the adhesion force between the metal and FTO glass.

There are limitations to our current method. Although LEIT is a cost-effective approach to replace vacuum-based metal deposition with an electroplating process for the fabrication of EMTEs, it comprises a mandatory lithography step when making each sample. This limits its suitability for high-throughput and large-volume industrial production. Our future work will be focused on addressing this important issue.

With better performance at a lower cost and the high-throughput fabrication strategy, our EMTE has a wide range of applications in flexible optoelectronic devices, such as organic solar cells[33], organic light-emitting diodes[34], organic thin-film transistors[35], flexible transparent touch panels[10], *etc*. Furthermore, the mesh can be used in artificial skin by transferring it to stretchable substrates. Currently, we are investigating its suitability in stretchable electronic devices. Indeed, its performance is promising in such applications.

In summary, we present novel EMTEs in which metal mesh is mechanically anchored in a polymer film. Compared to existing metal mesh electrodes, the key advantage of this EMTE structure is that it uses a thick metal mesh for higher electrical conductivity, without losing surface flatness. The EMTEs are fabricated to accomplish a ratio of electrical to optical conductance of more than 10^4, which is amongst the highest of the TEs[29] reported in literature. Furthermore, the embedded structure enhances the chemical stability of the EMTEs in an ambient atmosphere and the mechanical stability under bending stress.

Disclosures

The authors have nothing to disclose.

Acknowledgements

This work was partially supported by the General Research Fund of the Research Grants Council of the Hong Kong Special Administrative Region (Award No. 17246116), the Young Scholar Program of the National Natural Science Foundation of China (61306123), the Basic Research Program-General Program from the Science and Technology Innovation Commission of Shenzhen Municipality (JCYJ20140903112959959), and the Key Research and Development Program from the Zhejiang Provincial Department of Science and Technology (2017C01058). The authors would like to thank Y.-T. Huang and S. P. Feng for their help with the optical measurements.

References

1. Hecht, D. S., Hu, L., Irvin, G. Emerging Transparent Electrodes Based on Thin Films of Carbon Nanotubes, Graphene, and Metallic Nanostructures. *Adv Mater.* **23** (13), 1482-1513 (2011).
2. Bonaccorso, F., Sun, Z., Hasan, T., Ferrari, A. C. Graphene photonics and optoelectronics. *Nat Photonics.* **4** (9), 611-622 (2010).
3. Kirchmeyer, S., Reuter, K. Scientific importance, properties and growing applications of poly(3,4-ethylenedioxythiophene). *J Mater Chem.* **15** (21), 2077-2088 (2005).
4. Vosgueritchian, M., Lipomi, D. J., Bao, Z. Highly Conductive and Transparent PEDOT:PSS Films with a Fluorosurfactant for Stretchable and Flexible Transparent Electrodes. *Adv Funct Mater.* **22** (2), 421-428 (2012).
5. Zhang, M. *et al.* Strong, Transparent, Multifunctional, Carbon Nanotube Sheets. *Science.* **309** (5738), 1215-1219 (2005).
6. De, S. *et al.* Silver Nanowire Networks as Flexible, Transparent, Conducting Films: Extremely High DC to Optical Conductivity Ratios. *ACS Nano.* **3** (7), 1767-1774 (2009).
7. Groep, J., Spinelli, P., Polman, A. Transparent Conducting Silver Nanowire Networks. *Nano Lett.* **12** (6), 3138-3144 (2012).
8. Hong, S. *et al.* Highly Stretchable and Transparent Metal Nanowire Heater for Wearable Electronics Applications. *Adv Mater.* **27** (32), 4744-4751 (2015).
9. Bari, B. *et al.* Simple hydrothermal synthesis of very-long and thin silver nanowires and their application in high quality transparent electrodes. *J Mater Chem A.* **4** (29), 11365-11371 (2016).
10. Hyunjin, M., Phillip, W., Jinhwan, L., Seung Hwan, K. Low-haze, annealing-free, very long Ag nanowire synthesis and its application in a flexible transparent touch panel. *Nanotechnol.* **27** (29), 295201 (2016).
11. Lee, H. *et al.* Highly Stretchable and Transparent Supercapacitor by Ag-Au Core-Shell Nanowire Network with High Electrochemical Stability. *ACS Appl Mater Interfaces.* **8** (24), 15449-15458 (2016).
12. Cairns, D. R. *et al.* Strain-dependent electrical resistance of tin-doped indium oxide on polymer substrates. *Appl Phys Lett.* **76** (11), 1425-1427 (2000).
13. Bel Hadj Tahar, R., Ban, T., Ohya, Y., Takahashi, Y. Tin doped indium oxide thin films: Electrical properties. *J Appl Phys.* **83** (5), 2631-2645 (1998).
14. Kumar, A., Zhou, C. The Race To Replace Tin-Doped Indium Oxide: Which Material Will Win? *ACS Nano.* **4** (1), 11-14 (2010).
15. Hong, S. *et al.* Nonvacuum, Maskless Fabrication of a Flexible Metal Grid Transparent Conductor by Low-Temperature Selective Laser Sintering of Nanoparticle Ink. *ACS Nano.* **7** (6), 5024-5031 (2013).
16. Wu, H. *et al.* A Transparent Electrode Based on a Metal Nanotrough Network. *Nat Nanotechnol.* **8** (6), 421-425 (2013).
17. Han, B. *et al.* Uniform Self-Forming Metallic Network as a High-Performance Transparent Conductive Electrode. *Adv Mater.* **26** (6), 873-877 (2014).
18. Kim, H.-J. *et al.* High-Durable AgNi Nanomesh Film for a Transparent Conducting Electrode. *Small.* **10** (18), 3767-3774 (2014).
19. Kwon, J. *et al.* Low-Temperature Oxidation-Free Selective Laser Sintering of Cu Nanoparticle Paste on a Polymer Substrate for the Flexible Touch Panel Applications. *ACS Appl Mater Interfaces.* **8** (18), 11575-11582 (2016).
20. Suh, Y. D. *et al.* Nanowire reinforced nanoparticle nanocomposite for highly flexible transparent electrodes: borrowing ideas from macrocomposites in steel-wire reinforced concrete. *J Mater Chem C.* **5** (4), 791-798 (2017).

21. Bao, C. *et al.* In Situ Fabrication of Highly Conductive Metal Nanowire Networks with High Transmittance from Deep-Ultraviolet to Near-Infrared. *ACS Nano.* **9** (3), 2502-2509 (2015).
22. Osch, T. H. J., Perelaer, J., de Laat, A. W. M., Schubert, U. S. Inkjet Printing of Narrow Conductive Tracks on Untreated Polymeric Substrates. *Adv Mater.* **20** (2), 343-345 (2008).
23. Ahn, B. Y. *et al.* Omnidirectional Printing of Flexible, Stretchable, and Spanning Silver Microelectrodes. *Science*. **323** (5921), 1590-1593 (2009).
24. Khan, A., Rahman, K., Hyun, M.-T., Kim, D.-S., Choi, K.-H. Multi-nozzle electrohydrodynamic inkjet printing of silver colloidal solution for the fabrication of electrically functional microstructures. *Appl Phys A.* **104** (4), 1113-1120 (2011).
25. Khan, A., Rahman, K., Kim, D. S., Choi, K. H. Direct printing of copper conductive micro-tracks by multi-nozzle electrohydrodynamic inkjet printing process. *J Mater Process Technol.* **212** (3), 700-706 (2012).
26. Ellmer, K. Past achievements and future challenges in the development of optically transparent electrodes. *Nat Photonics.* **6** (12), 809-817 (2012).
27. Choi, H.-J. *et al.* Uniformly embedded silver nanomesh as highly bendable transparent conducting electrode. *Nanotechnol.* **26** (5), 055305 (2015).
28. Khan, A., Li, S., Tang, X., Li, W.-D. Nanostructure Transfer Using Cyclic Olefin Copolymer Templates Fabricated by Thermal Nanoimprint Lithography. *J Vac Sci Technol B.* **32** (6), 06FI02 (2014).
29. Khan, A. *et al.* High-Performance Flexible Transparent Electrode with an Embedded Metal Mesh Fabricated by Cost-Effective Solution Process. *Small.* **12** (22), 3021-3030 (2016).
30. Moon Kyu, K., Jong, G. O., Jae Yong, L., Guo, L. J. Continuous phase-shift lithography with a roll-type mask and application to transparent conductor fabrication. *Nanotechnol.* **23** (34), 344008 (2012).
31. Chou, S. Y., Krauss, P. R., Renstrom, P. J. Imprint of sub-25 nm vias and trenches in polymers. *Appl Phys Lett.* **67** (21), 3114-3116 (1995).
32. Manfrinato, V. R. *et al.* Resolution Limits of Electron-Beam Lithography toward the Atomic Scale. *Nano Lett.* **13** (4), 1555-1558 (2013).
33. Khan, A. *et al.* Solution-processed Transparent Nickel-mesh Counter Electrode with In-situ Electrodeposited Platinum Nanoparticles for Full-Plastic Bifacial Dye-sensitized Solar Cells. *ACS Appl Mater Interfaces.* (2017).
34. Lee, J. *et al.* A dual-scale metal nanowire network transparent conductor for highly efficient and flexible organic light emitting diodes. *Nanoscale.* **9** (5), 1978-1985 (2017).
35. Khan, S. *et al.* Direct patterning and electrospray deposition through EHD for fabrication of printed thin film transistors. *Current Appl Phys.* **11** (1), S271-S279 (2011).

